# Tailoring hydroxyapatite microspheres by spray-drying for powder bed fusion feedstock

Pedro Navarrete-Segado, Christine Frances, David Grossin, Mallorie Tourbin

Powder Technology 398 (2022) 117116

Contents lists available at ScienceDirect

Powder Technology

journal homepage: www.elsevier.com/locate/powtec

# Tailoring hydroxyapatite microspheres by spray-drying for powder bed fusion feedstock

P. Navarrete-Segado [a,b], C. Frances [b], D. Grossin [a], M. Tourbin [b,*]

[a] CIRIMAT, Université de Toulouse, CNRS, 4 Allée Émile Monso, 31432 Toulouse Cedex 4, France
[b] Laboratoire de Génie Chimique, Université de Toulouse, CNRS, 4 Allée Émile Monso, 31432 Toulouse Cedex 4, France

ARTICLE INFO

*Article history:*
Received 23 September 2021
Received in revised form 2 January 2022
Accepted 4 January 2022
Available online 10 January 2022

*Keywords:*
Hydroxyapatite
Microspheres
Spray-drying
3D printing
Flowability
Powder bed fusion

ABSTRACT

The present work deals with a study on the physical characteristics of stoichiometric hydroxyapatite microspheres produced by spray-drying process through different operating conditions. Obtained hydroxyapatite microspheres are intended to be used as powder feedstock in powder bed selective laser processing additive manufacturing technologies where the flowability and the particle size distribution of the powder feedstock are of special importance. The powders produced at different spray-drying operating parameters were evaluated by analysing the particle size, shape, moisture, and agglomerates strength. Spray air pressure (0.25–2 bars) and the solid content of the slurries (10–50% wt.) were the most influent parameters to control the final particle size distribution, whereas the higher process recovery rate (79%) was obtained at specific values of inlet temperature (250 °C), spray air pressure (2 bar), and feed rate (4.9 $kg.h^{-1}$). A 5 wt% of polyvinyl alcohol as an organic binder to the ceramic part was found to increase the strength of the granules. The flowability of the produced hydroxyapatite microspheres ($x_{50}$ = 64 μm; span = 1.77) was found to fulfil the defined feedstock requirements (e.g., Hausner ratio < 1.25), without alteration of the physico-chemical properties of the material. These promising results confirm the use of a spray dryer as an efficient method for the production of hydroxyapatite microspheres for powder bed selective laser processing.



## 1. Introduction

Spray-drying (SD) process is one of the many methods proposed for the production of ceramic particles with controllable morphology, from which we can distinguish bottom-up (precipitation, supercritical fluid…) and top-down (mechanical milling, freeze-drying…) processes [1]. While with SD is possible to produce and tailor already existing particles into high-purity spherical shape ceramic agglomerates in an economical, continuous, and rapid way [2]. SD technique transforms liquid state feed into dried particulate form by spraying the feed into a hot drying medium. The feed can be constituted of a suspension, emulsion, or solution. In addition, it is common to use additives, such as dispersants and binders, to control the stability of the particles against flocculation and the hardness of the resulting particles. The final product morphology depends on several factors, including the physical and chemical properties of the feed formulation, process conditions, and the equipment geometry [2,3].

The advantages of a SD process, such as particle size distribution (PSD) and morphology control, make it an interesting option for the production of microspheres composed of hydroxyapatite (HA), a very well-known bio-ceramic material in bone tissue engineering because of its ideal properties for bone tissue reparation [4–6]. It has chemical similarity to bone and its high bioactivity, biocompatibility, and stability ensure good osseointegration of the implants while maintaining good mechanical and chemical resistance [7]. The recent application of Additive Manufacturing (AM) technologies to process ceramic materials open new ways to produce ceramics for many diverse applications (healthcare, aerospace…). Precisely the Powder Bed Selective Laser Processing (PBSLP) method uses a laser to sinter/melt selectively regions of a ceramic powder bed fabricating parts from previously designed 3D models [8]. The production of HA parts for tissue engineering and implantology has been possible through the use of composites comprising biocompatible polymers such as poly-L-lactic acid (PLLA), polycaprolactone (PCL), and poly(3-hydroxybutyrate-*co*-3-hydroxyvalerate (PHBV)) as the main component [9–12]. However, some research is still needed on the direct use of pure HA as powder feedstock, or at least as main component, for the production of parts that could wholly benefit from the ideal properties for bone tissue reparation of this calcium phosphate-based bio-ceramic [13–15].

When tailoring the powder feedstock properties for PBSLP method it is important to know the needs required for optimal performance during the process. Microstructural composition, physico-chemistry

* Corresponding author.
*E-mail address:* mallorie.tourbin@ensiacet.fr (M. Tourbin).

https://doi.org/10.1016/j.powtec.2022.117116

**Abbreviation**

| | |
|---|---|
| AM | Additive manufacturing |
| FTIR | Fourier-transform infrared |
| HA | Hydroxyapatite |
| Ham | Hydroxyapatite microspheres |
| PBSLP | Powder bed selective laser processing |
| PCL | Polycaprolactone |
| PSD | Particle size distribution |
| PVA | Polyvinyl alcohol |
| SD | Spray drying |
| SEM | Scanning electron microscopy |
| XRD | X-ray diffraction |

*Symbols*

$\dot{\gamma}$ = Shear rate [$s^{-1}$]
$A_{UCT}$ = cross-sectional section area of the mould [$mm^2$]
$f_c$ = Unconfined yield strength [Pa]
$ff_c$ = Flowability coefficient / flow factor coefficient [−]
K = Consistency index [$Pa.s^n$]
n = flow index [−]
N = Total number of replicate measurements
$N_c$ = Normal load [Pa]
$N_f$ = Normal force at specimen failure [Pa]
P = Spray air pressure [bar]
Qs = Feed rate [$kg.h^{-1}$]
$R^2$ = Correlation ratio [−]
$T_{int}$ = Inlet temperature [°C]
$w_{HA}$ = Hydroxyapatite solid mass fraction [−]
$x_{10}$ = The 10th percentile [μm] (diameter of a sphere at which 10% of the particles in the sample are smaller)
$x_{50}$ = Median particle size [μm] = the 50th percentile (diameter of a sphere at which 50% of the particles in the sample are smaller)
$x_{90}$ = The 90th percentile [μm] (diameter of a sphere at which 90% of the particles in the sample are smaller)
$\eta$ = Viscosity [Pa.s]
$\sigma_1$ = Consolidation stress [Pa]
$\tau$ = Shear stress [Pa]

rheology, thermal, and optical properties should be tailored to improve printed parts quality [16,17]. One of the PBSLP method steps makes use of a recoater to repeatedly spread the powder homogeneously on the building platform creating thickness-controlled powder beds before the laser scanning. Powder feedstock flowability and packing density are then crucial properties for their processability, and these can be tuned by modifying the powder morphology (shape and size) and size distribution. One measurement method for powder flowability is the ratio of tap and bulk density (Hausner ratio) [18]. A PBSLP powder feedstock should yield a Hausner ratio of less than 1.25**.** This is better achieved by flowable spherical agglomerates particles within the micron range ($x_{50}$ > 20 μm) [8,19–22]. In addition, the use of polydisperse size distribution (span >1) has demonstrated to improve their flowability and packing density, with the smaller particles filling the interstitial void between larger particles [23–25]. It makes the SD an excellent process for the production of hydroxyapatite microspheres (HAm) intended for PBSLP, since the possibility of controlling their PSD as well as the morphology allows the tailoring of powders properties such as flowability and packing density.

A growing interest in the production and employment of HAm on diverse applications, including AM technologies [26–28] and biomedical fields [29–32], can be observed in an increase in the number of research works focused on these materials during the most recent years. Though it can be observed that not many studies are focused on the production of HAm through SD, nor on the evaluation of the experimental conditions on the final dried HAm properties (e.g., flowability). Some recent examples have been offered by Bastan [5], Yang and Wang [33], Chow [34], and Schappo [35]; however, these works do not cover completely the large variety of parameters affecting the final powder properties (slurry formulation, operating conditions, apparatus geometry…) for hence, there is still then a need to extend the research in this topic.

The goal of the present study would be, first, the preparation of the HA slurries meeting the expected properties in terms of rheology and stability for their processing by SD (this part was mainly covered in another work). Then, we will focus on the evaluation of the effect of the slurry formulation and operating parameters during the SD process on the final HAm powder properties. The main objective will be then the production of HAm powder with a targeted particle size in the micron range (30 μm < $x_{50}$ < 70 μm) and a certain size polydispersity (span >1) to fulfil the flowability requirements (e.g., Hausner ratio < 1.25) for its use in a PBSLP process [36].

## 2. Materials and method

### 2.1. Materials

Stoichiometric hydroxyapatite (HA) aqueous slurries used during the present study were produced by stirred bead milling process. Once the objective initial particle size range ($x_{50}$ = 0.2–1.5 μm) was reached by wet milling, the influence of the HA load and the dispersant dosage in the viscosity of the slurry was studied since the higher is the load content of a suspension the less is the amount of water needed to be dried, thus increasing the process efficiency. First, a suitable dispersant able to produce the deflocculation of the HA particles and hence increase the suspension stability was found. The ammonium polymethacrylate dispersant, named Darvan C and provided by R. T. Vanderbilt Co. (Norwalk, CT, USA) was assessed. The optimum dispersant dosage was determined in terms of viscosity, zeta potential, and sedimentation speed measurements. It was a concentration of 2.1 $mg/m^2$ of dispersant active matter with respect to the ceramic surface or what is the same, a 5 wt% respect to the ceramic powder mass. Secondly, the highest processable HA load in a suspension was found to be a solid mass fraction ($w_{HA}$) of 0.5, that is to say the 50% of the total mass of the suspension. Following this previous study, all suspensions used in the present work contain a 5 wt% of dispersant DC and a solid content of HA $w_{HA}$ = 0.5 was preferred even if the influence of lowering the load content on the final HAm properties was assessed. Thus, in this work only the effect of the binder addition on the slurry stability was studied.

Polyvinyl alcohol (PVA), Rhodoviol® 8/140 was obtained from VWR Chemicals® and was used as an organic binder during the spray-drying process for its excellent granulation properties. PVA granules were dissolved in water at 90 °C (20 wt% granules, 80 wt% distilled water) to prepare a homogeneous solution before adding it to the respective HA powder slurries.

Two additional powders were evaluated for flowability comparison with the spray-dried powder produced in the present work:

- First, a commercial HA powder from the company Urodelia® S.A (ref. 300–08-2) was used as reference material of powder that already showed promising results in terms of flowability in a PBSLP apparatus.
- The HA powder of the initial slurries was filtered and dried at 70 °C overnight obtaining an initial HA powder for comparison of flowability.

### 2.2. Characterization of the powders and slurries

#### 2.2.1. Morphological and structural properties of the particles

All PSD of HA suspensions and dry powders were performed with a Mastersizer MS 3000 (Malvern Panalytical®) laser particle size analyser

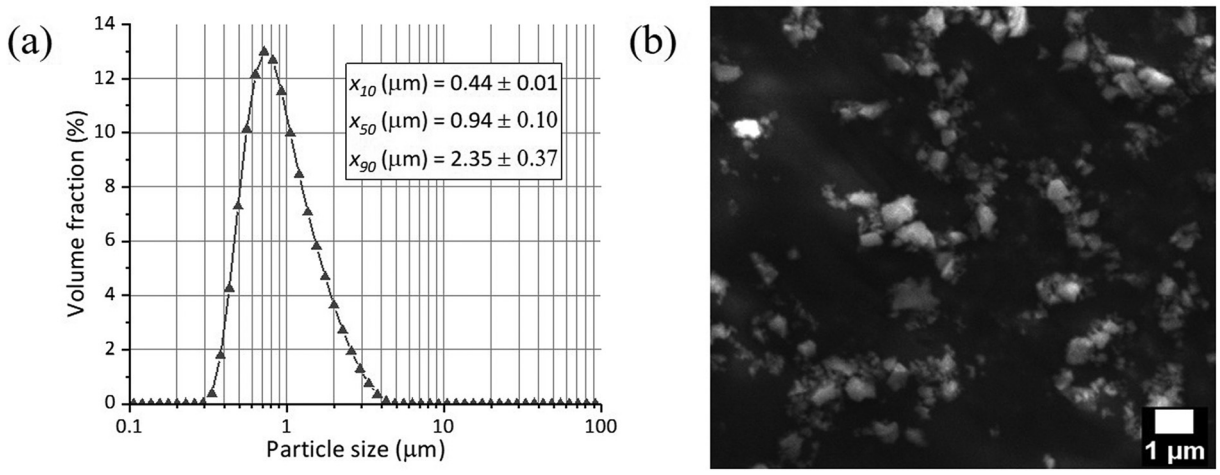


**Fig. 1.** (a) PSD of the primary stoichiometric hydroxyapatite powder measured in dispersion. (b) SEM micrograph of the same dried powder.

(refractive indexes: 1.63 and 1.33 for particles and water, respectively; dispersion pressure of 0.1 bar and a standard stainless steel venturi disperser for dry powders). A total number of replicate measurements (N) of five was performed for each measurement to calculate the resulting sample mean and sample standard deviation. Obtained values will be given as follows: mean ± standard deviation.

Whenever it is possible to replicate the measurements, the majority of the analytical results in this publication will be given in the form (N, mean ± standard deviation).

The morphology of powders present in this work was investigated with a scanning electron microscope (SEM) LEO 435 VP (Leica®) equipped with a Ge detector (Imix-PC, Princeton Gamma-Tech) and metallization of the ceramic surface was performed with a thin film of silver using a Scancoat Six sputter coater. Particle size distribution of the initial HA slurry and SEM micrographs of the particles (dried) constituting of the initial suspension, can be observed in Fig. 1.

The specific surface of these initial particles was found to be 23.81 ± 6.00 $m^2.g^{-1}$. Determined in a Micromeritics® TriStar II Plus 3.00 equipment through physisorption analysis of overnight freeze-dried powder ($N = 3$). Ultrapure water used as dispersion medium was produced by the equipment "Purelab Ultra" of VWS (UK) Ltd. The water density was measured at 25 °C obtaining 0.99 $g.cm^{-3}$, whereas its pH varied between 6.3 and 6.8 at 25 °C.

### 2.2.2. Chemical and structural analyses

Fourier transform infrared spectroscopy (FTIR) analysis performed with a spectrometer FTIR Nicolet iS50 (Thermo Fischer Scientific) and the KBr pellet method was used to determine the composition of the powder before and after the spray-drying process. About 9 mg of sample powder were homogeneously stirred in a clean mortar to mix it with dry KBr powder (300 ± 5 mg). A compression load of 6000 kg was used to produce the analysed sample pellets. FTIR spectra was measured from the pellet in a 4000–400 $cm^{-1}$ wavenumber range with a step width of 0.48 $cm^{-1}$.

Thereafter, X-ray diffraction (XRD) analysis was performed by BRUKER's X-ray diffractometer D8 by using Cu Kα radiation (wavelength λ = 0.15406 nm) with a nickel filter at 40 kV and 40 mA. Samples diffractograms were recorded in a 2θ range between 20° and 90°, with a step of 0.03° 2θ, and a time per step of 0.2 s.

### 2.2.3. Rheological behaviour

Rheological analyses were undertaken to study the PVA binder influence on HA slurries viscosity and stability. These analyses were performed in a TA Instruments® AR2000 rheometer using a 40 mm crosshatched parallel plates system with a gap equal to 1300 μm and a Peltier plate. The measurements were performed with a conditioning step at a shear rate of 200 $s^{-1}$ during 30.0 s and an equilibration time of 30.0 s. Steady-step shear flow curves were then obtained for each sample at a constant plate temperature of 25 °C and an increasing shear rate in the range of 1–1000 $s^{-1}$ by taking ten data points by decade. This range includes the pumping and mixing processes typical ranges of shear rate to which the suspensions will be exposed during the spray-drying process [37]. Power Law model was found to fit properly the rheological analyses data for those suspensions.

### 2.2.4. Suspension stability analyses

Additionally, to support our study on the HA slurries stability before drying, electrophoretic analyses were performed to determine their zeta potential depending on the amount of PVA binder. A Zetasizer Nano-ZS (Malvern Panalytical®) was employed for the analyses at a constant temperature of 25 °C. Samples were diluted and adjusted to a concentration of 4 $mg.mL^{-1}$ before the analysis to avoid the multiple diffusion phenomena.

### 2.2.5. Powder flow experiments

Powder flow experiments of initial, spray-dried, and commercial powders were conducted following the standardized methods, specifications, and comments raised by the European Pharmacopoeia Chapter 2.9.36. A brief explanation for each of the five different flowability tests used in this work is presented below:

- Angle of repose, is the angle formed by the pile powder (relative to the horizontal) when it is poured through a funnel. It is a characteristic related to interparticle friction or resistance to movement between particles. Some variation in the qualitative description of powder flow using the angle of repose exists, however authors seem to agree with the classification given by Carr [38]. According to this classification, for good or even excellent flowability, the powder must present an angle of repose between 25° to 35°.
- Compressibility index and Hausner ratio are closely related and both have become the most simple, fast, and popular methods to predict the powder flow behaviour. Both are determined by measuring the bulk ($\rho_0$) and tapped ($\rho_f$) densities of powders. They are calculated as follows:

$$Compressibility\ index = 100 * \left(\frac{\rho_0 - \rho_f}{\rho_0}\right) \quad (1)$$

$$Hausner\ ratio = \frac{\rho_0}{\rho_f} \quad (2)$$

The largely accepted scale of flowability is given in European Pharmacopoeia Chapter 2.9.36. For good or even excellent flowability, the compressibility index of the powder must be lower or equal to 15% and the Hausner index must be under 1.25 [16].

- The flow through an orifice, has been proposed as the best measure of flowability of free-flowable powders [39]. It is measured as the mass per time flowing from any of a number of types of containers (cylinders, funnels, hoppers). There is no general flowability scale available since the flow rate is dependent on the method used to measure it. Comparison between different published results is then difficult. Experimental studies have detected a significant influence of orifice height on powder mass flow rate, thus for better comparison of the experimental results information regarding the orifice height used should always be referred [39].
- The flow factor coefficient of powders ($ff_c$) is used as a flowability index according to the classification by Jenike [40]. The flowability of a bulk solid can be characterized by its unconfined yield strength, $f_c$, in dependence on consolidation stress, $\sigma_1$. Usually, the ratio $ff_c$ of consolidation stress, $\sigma_1$, to unconfined yield strength, $f_c$, is used to characterize flowability numerically. The larger the $ff_c$ is, the better a bulk solid flows. For easy or free flowing of the powder, the flow factor must be higher than 4.

The following paragraphs contain more detailed information about the procedures followed and the equipment used for each of the five flowability tests performed:

- The angle of repose, compressibility index (eq. (1)), and Hausner ratio (eq. (2)) of the powders were evaluated on a powder characteristics tester PT-S (Hosokawa Micron B. V®).
- The flow rate of the different powders was measured in discrete samples by measuring the time it tooks for 100 g of powder to pass through the orifice of a stemless funnel (truncated cone) to the nearest tenth of a second. A glass funnel with an inner diameter of 15.5 cm, 13.5 cm height and a circular orifice diameter of 3.2 cm was used as container. Then, the orifice was circular and free of any vibration. The use of a stemless funnel was preferred instead of one with stem to avoid any effect of the friction between the stem and the flowing powder.
- The $ff_c$ ratio was measured in a universal mechanical testing press Hounsfield H25KS (Tinius Olsen®, USA) following the procedure described by Poletto et al. [41]. Once the cylindrical mould (diameter of 8.3 mm) was filled with 1 g of powder sample, the piston is moved downwards applying a normal load, $N_c$, of 75 MPa with a speed of 20 mm.min$^{-1}$. The compression step is carried with the piston moving downwards with a speed of 1 mm.min$^{-1}$ onto the consolidated sample increasing the normal force, until reaching the normal force at specimen failure, $N_f$. The flow factor ($ff_c$) is then calculated as the ratio between the major principal stress at steady state, $\sigma_1$, and the unconfined yield strength, $f_c$. Both calculated in turn following the equations below:

$$\sigma_1 = \frac{N_c}{A_{UCT}} \quad (3)$$

$$f_c = \frac{N_f}{A_{UCT}} \quad (4)$$

Where $A_{UCT}$ is the cross-sectional area of the mould (54.11 mm$^2$).

At least six measurements ($N = 6$) were recorded to obtain the standard deviations of the means for the angle of repose, compressibility index, Hausner ratio, and flow rate, then at least three measurements ($N = 3$) to obtain the standard deviation of the mean for $ffc$ of each powder.

### 2.3. Spray-drying experiments

The spray-drying process was carried out in an APV Anhydro (SPX Flow®, USA) 1-m diameter chamber pilot spray-drying plant (Fig. 2), model PSD 52 in 316 stainless steel. The process starts with the HA slurry being pumped from the bottom of the chamber by means of a BOYSER® peristaltic pump (model AMP-10/B) while stirred with a Heidolph instruments® mechanical stirrer equipped with a straight-blade impeller at 150 rpm. Then, the slurry was finely sprayed into the chamber through a SU04 two-fluid external mixing nozzle (Fluid Cap 60,100 + Air Cap 120) from Spraying Systems Co. ® with round spray pattern in a 17–19° spray angle. An air duct heater produces a stable heating of the chamber drying the drops into powder, then a flow (125 m$^3$.h$^{-1}$) is created by an aspirator, to lead the powder reaching the cyclone where the solid particles are separated from the air flow and settled into a collection jar. Once the powder is separated, the air loaded with very fine particles passes through a filter bag in order to minimize the fine particles emissions. The list of experimental runs performed for the present study together with the slurry formulation, experimental conditions, and results information can be found in Table 1.

The experimental runs were carried out following the methodology below:

- Run 1: The objective of this run was to evaluate, using "standard" experimental conditions, the steady state regime of the equipment, as well as the global performance of the process (recovery rate, residual powder moisture, PSD…) and the operation time needed for the rest of the study.
- Runs 2–14: Through these runs, we could examine the influence of the slurry formulation and the experimental conditions on the final powder properties. It also allowed us to find the set of parameters producing the powder that better meet the properties needed for its use in a PBSLP process.

The procedure followed for the runs started with the operating parameters of the SD process being settled by using water as feed. Thus, reaching an estimated temperature of the chamber before start pumping the suspension. Once the process finished the powder inside of the collection jar was extracted and stocked for analysis. In the case of the Run 1 (operation time study) the cyclone valve was closed every ten minutes and the powder inside of the container was collected and stocked for analysis. Then, the recipient was returned to the cyclone and the valve was reopened to continue collecting the product.

Powders obtained were weighted for recovery rate studies and analysed for their water content with a commercial moisture analyser (MBT 64 M-C model from VWR®). A standard drying profile was used to dry the powder to constant weight at 110 °C.

## 3. Results and discussion

### 3.1. Preparation of HA slurry properties

The preparation of the highly-loaded aqueous HA slurries already started with the diminution of the particle size in a sub-micron range ($x_{50}$ = 0.2–1.5 μm) by wet grinding of the suspensions. A series of studies demonstrated a higher heat transfer efficiency and more solid, dense and spherical microspheres are obtained when using ceramic primary particles having with a median particle size, $x_{50}$, in the range of 0.2 to 1.5 μm [42–45]. Then, preliminary tailoring of the particle size was preferred prior spray-drying process.

Depending on the application, spray-dried spherical granules with controlled hardness and deformability may be required. We can find

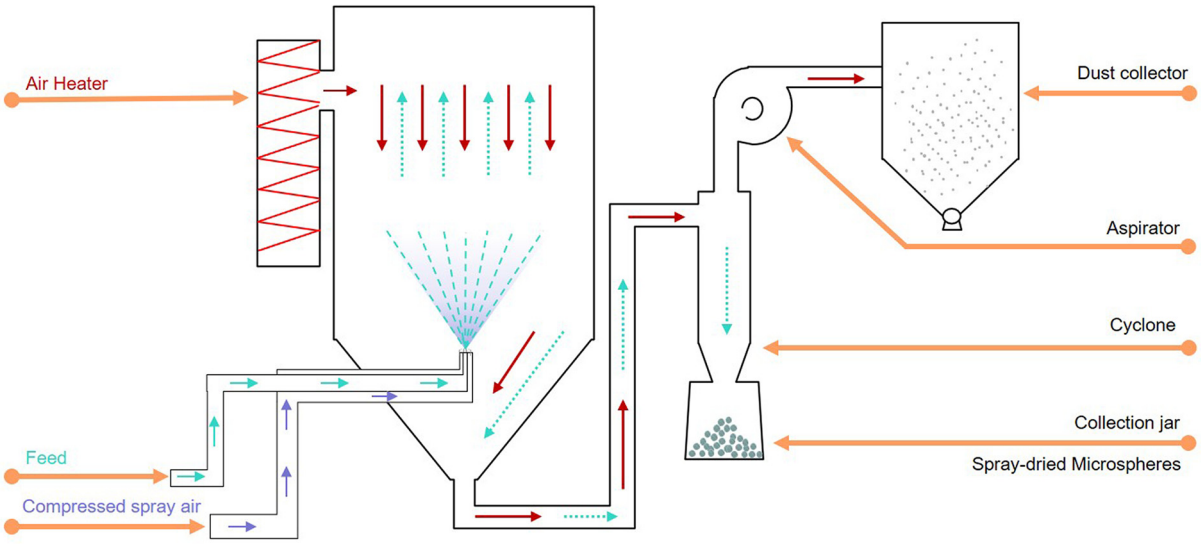


**Fig. 2.** Schematic representation of the pilot-scale spray dryer.

some works studying the effect of adding different organic binders to the ceramic suspension on the final granule characteristics [46,47]. However, the use of a binder can induce an increase in the slurry viscosity and produce the destabilization of an already dispersant-stabilized suspension. In a PBSLP process the importance of having coherent granules or not has not been studied yet. Some PBSLP apparatus are equipped with a cylindrical recoater part that is able to produce a compression of the powder bed once it has been spread. Further research is needed to know if the packing density of the powder bed is improved by using easy-deformable granules or not at the moment of compress it. In the present study, suspensions with and without binder in their composition were spray-dried and its influence on the final HAm characteristics (morphology and strength) was analysed.

The effect of the addition of the binder PVA on the dispersant-stabilized slurries was determined through viscosity and zeta potential measurements. Three similar volumes of aqueous solutions, two of them containing 3 and 5 wt% of binder PVA (respect to the ceramic powder) were prepared and poured to three different samples of a HA suspension at $w_{HA} = 0.3$ to study the binder influence on the viscosity. Fig. 3a shows the shear stress versus shear rate diagram of the HA suspensions at different PVA concentrations. The best-fit parameter values of these rheograms by a power-law of type $\tau = K(\dot{\gamma})^n$ with $\tau$ the shear stress [Pa], $\gamma$ the shear rate [$s^{-1}$], K the consistency index [Pa.$s^n$] and n the flow index [−] can be observed in Table 2. All suspensions analysed exhibited pseudoplastic behaviour over the whole shear rate range, also confirmed by the flow behaviour indexes (n being less than 1). It is important to note that the correlation ratios, $R^2$, indicate that the Power Law model fits the measurements well.

The viscosity of aqueous suspensions with different PVA concentrations is compared in Fig. 3b. As expected, the higher the PVA concentration, the higher the slurry viscosity is. However low viscosity values were observed, even for high binder concentration (< 0.1 Pa.s for the whole shear rate range). These results are in agreement with those of Tsetsekou et al. [42] who observed that the addition of PVA binder into alumina slurries exhibited a slight increase of the viscosity. A higher PVA content may increase the resistance to deformation by shear stress due to the presence of more entities in the suspension reducing the free space for individual particles to move around.

**Table 1**
List of spray-drying experiments performed, including the slurry formulation, experimental conditions, and resulting powder properties. $w_{HA}$ = HA solid mass concentration, $T_{int}$ = inlet temperature, P = spray air pressure, Qs = feed rate (for all experiments, the drying air flow rate is kept constant at 125 $m^3.h^{-1}$).

| | Formulation | | | Experimental conditions | | | Result | | | | | | |
|---|---|---|---|---|---|---|---|---|---|---|---|---|---|
| Run N° | $w_{HA}$ (−) | DC conc. (wt% of active matter) | PVA conc. (wt%) | $T_{int}$ (°C) | $P$ (bar) | $Qs$ ($kg.h^{-1}$) | $x_{10}$ (μm) | $x_{50}$ (μm) | $x_{90}$ (μm) | Recovery rate (%) | Span (−) | Moisture content (%) | Parameters effect studied |
| 1 | 0.5 | 5 | 0 | 250 | 0.25 | 3.2 | 25 ± 7 | 64 ± 4 | 123 ± 1 | 37 | 1.77 | 1.5 | "standard" experimental conditions |
| 2 | 0.1 | 5 | 0 | 250 | 0.25 | 3.2 | 10 ± 2 | 27 ± 2 | 61 ± 2 | 32 | 1.78 | 1.1 | $w_{HA}$ |
| 3 | 0.3 | 5 | 0 | 250 | 0.25 | 3.2 | 16 ± 3 | 47 ± 2 | 88 ± 0 | 22 | 1.38 | 1.3 | $w_{HA}$ |
| 4 | 0.5 | 5 | 0 | 250 | 0.25 | 4.9 | 56 ± 4 | 88 ± 3 | 137 ± 2 | 23 | 0.81 | 1.6 | $Qs$ |
| 5 | 0.5 | 5 | 0 | 250 | 0.25 | 5.8 | 72 ± 2 | 101 ± 2 | 140 ± 5 | 19 | 0.64 | 1.8 | $Qs$ |
| 6 | 0.5 | 5 | 0 | 250 | 1 | 3.2 | 29 ± 4 | 58 ± 2 | 101 ± 2 | 24 | 1.56 | 1.6 | $P$ |
| 7 | 0.5 | 5 | 0 | 250 | 2 | 3.2 | 16 ± 3 | 45 ± 1 | 88 ± 2 | 46 | 1.93 | 1.4 | $P$, $Qs + T_{int}$ |
| 8 | 0.5 | 5 | 3 | 250 | 0.25 | 3.2 | 44 ± 4 | 78 ± 5 | 131 ± 6 | 20 | 1.15 | 3.8 | PVA conc. |
| 9 | 0.5 | 5 | 5 | 250 | 0.25 | 3.2 | 30 ± 3 | 65 ± 4 | 117 ± 6 | 19 | 1.37 | 4.6 | PVA conc. |
| 10 | 0.5 | 5 | 0 | 275 | 0.25 | 3.2 | 27 ± 8 | 66 ± 2 | 122 ± 2 | 16 | 1.21 | 1.4 | $T_{int}$ |
| 11 | 0.5 | 5 | 0 | 300 | 0.25 | 3.2 | 30 ± 8 | 87 ± 10 | 221 ± 12 | 18 | 1.99 | 1.2 | $T_{int}$ |
| 12 | 0.5 | 5 | 0 | 250 | 2 | 4.9 | 8 ± 0 | 31 ± 0 | 75 ± 1 | 79 | 2.15 | 2.0 | $Qs + T_{int}$ |
| 13 | 0.5 | 5 | 0 | 300 | 2 | 9.7 | 9 ± 0 | 38 ± 1 | 101 ± 3 | 76 | 2.34 | 2.3 | $Qs + T_{int}$ |
| 14 | 0.5 | 5 | 0 | 320 | 2 | 11.3 | 10 ± 1 | 40 ± 1 | 100 ± 2 | 75 | 2.17 | 1.9 | $Qs + T_{int}$ |

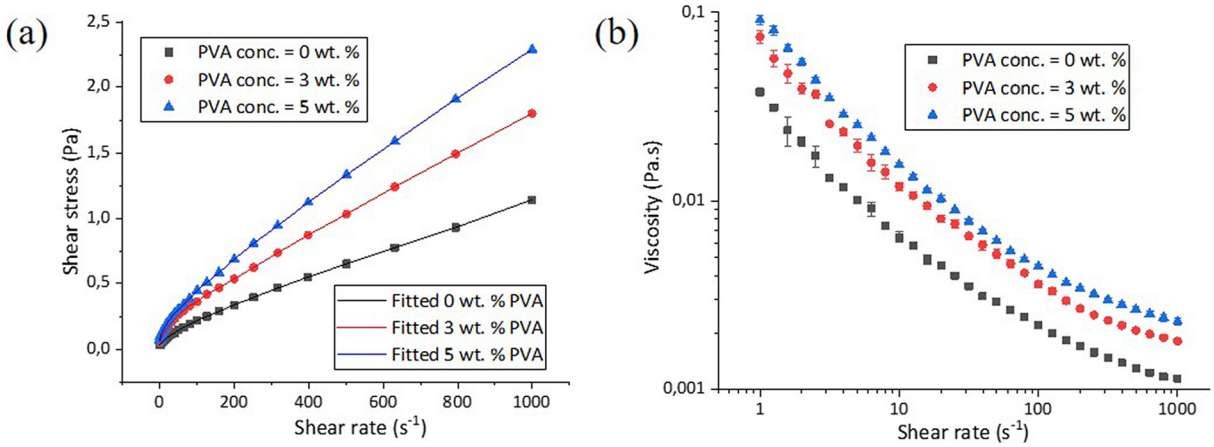


**Fig. 3.** (a) Flow data for several suspensions containing different binder concentrations fitted to the Power Law model and (b) viscosity-shear rate curves.

In addition, the zeta potential evolution of the HA suspensions was analysed in the PVA dosage range of 0–5 wt% relative to the HA content. The addition of PVA can alter the slurry stability, reducing the zeta potential of the slurries and producing the pre-agglomeration of the particles in suspension that could preclude a correct formation of the dry agglomerates during the SD process. It is commonly accepted that for aqueous suspensions, a zeta potential value lower than −30 mV (or higher than 30 mV) indicate a good stabilization of the suspension [48]. Then, it was important to avoid the alteration and increase of the zeta potential of the suspension over this limit value. Fig. 4 shows the average of the zeta potential values from a set of five measurements for each of the three analysed suspensions. It can be observed how the suspension was already well stabilized due to the previous addition of DC. Between the suspensions containing PVA, the one with a 5 wt% of PVA respect to the ceramic showed a lower value for the zeta potential of the suspension indicating a lower alteration of the initial stability of the slurry. In this section it was demonstrated that the addition of PVA to the slurries prior to the SD process induced a higher but controlled slurry's viscosity.

This section demonstrated that the addition of PVA to the slurries prior to the SD process induced a higher but controlled slurry's viscosity. In addition, comparing these concentrations, a concentration of 5 wt% of PVA respect to the ceramic kept a higher stability of the suspensions with a lower zeta potential value.

### 3.2. Spray-drying of the HA suspension

Below, the time to reach a steady-state regime and the effect of the operating parameters of the SD continuous process on the final HAm properties are analysed. Different experiment runs where performed with diverse parameters combinations. These operating parameters were the feed rate, solid mass fraction, spray air pressure, inlet temperature, and the binder dosage. The influence of these parameters has been investigated in terms of resulting PSD and particles shape through SEM micrographs analyses of the produced HAm and residual moisture content of the powder after drying.

**Table 2**
Parameters fitted to Power Law model for HA suspensions with different PVA concentrations in steady-state conditions during the shear stress-shear rate test (imposed shear range 1–1000 $s^{-1}$).

| | | PVA conc. (wt%) | | |
|---|---|---|---|---|
| Sample | | 0 | 3 | 5 |
| Consistency index $K$ [$10^{-3}$ Pa.s$^n$] | Value | 9 | 18 | 21 |
| | Standard Error | 0.90 | 2.24 | 2.47 |
| Flow index n | Value | 0.69 | 0.66 | 0.67 |
| | Standard Error | 0.01 | 0.02 | 0.02 |
| Correlation ratio $R^2$ | | 0.99 | 0.98 | 0.99 |

#### 3.2.1. Steady-state regime

Firstly, the time to reach the steady-state process regime in which the variables remain constant as time changes was evaluated in the conditions described for the run 1. Fig. 5a shows the average particle size obtained at different process times. A certain variation of the particle size is observed within the time of the experiment but not a clear tendency can be perceived. Assuming that the time required to bring the equipment up to operating capability under these conditions is no more than two hours (time over which the process has been monitored), it would indicate that the steady-state of the process is reached rapidly at the beginning of the experiment and that not important variations for the particle size of the powder obtained are expected. As was already indicated in Table 1, the average $x_{10}$, $x_{50}$, and $x_{90}$ of the whole process are 17.5 μm, 57.0 μm, and 121.4 μm with standard deviations of ±4.01 μm, ± 7.08 μm, and ± 6.69 μm respectively. The evolution of the product quality with the process time is also observed in the evolution of the PSD of the powders shown in Fig. 5b. A certain difference is perceived between distributions but neither here a clear variation tendency depending on the process time is observed. All powders showed a roughly similar PSD span.

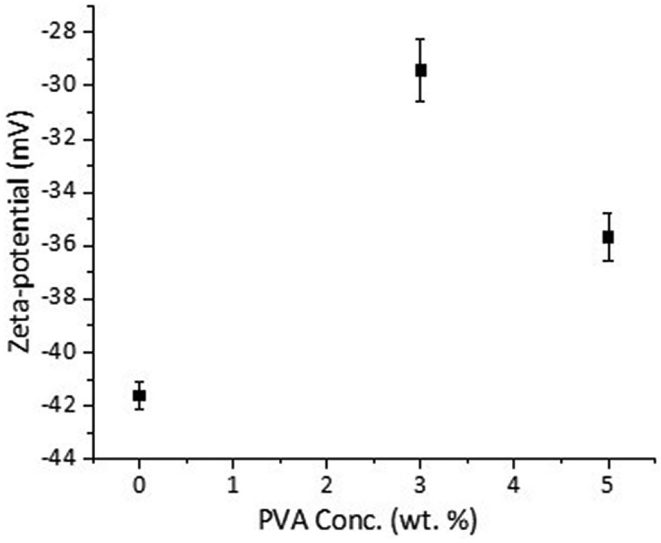


**Fig. 4.** Effect of PVA dosage on HA dispersant-stabilized slurries zeta potential.

HAm morphologies at different process time can be seen on Fig. 6. The majority of the particles had small rough spherical and dense morphology, produced by the use of submicronic particles (much smaller than the size of droplets) as starting material. The spherical particles have almost no external visible porosity in their structure. Other particle morphologies can also be observed in the SEM micrographs but in a very lesser extent (Fig. 7). These are doughnut, convex, and mushroom particle morphologies produced by the hydrodynamics, the structural stability, and the behaviour of the droplets transforming the spherical droplet into other forms [2,49]. This droplet transformation happens at specific process conditions (e.g., too high temperature process, presence of surfactants…). Okuyama et al. [2] found in their study that doughnut type particles had higher surface area, lower density and more than a 30% of porosity than spherical dense particles.

Formation mechanisms of dense small rough spherical dense particles, as well as, mushroom, convex, and doughnut particles are illustrated in Fig. 7a and Fig. 7b, respectively. In addition, the SEM micrographs of individual spray-dried HAm, doughnut HA particle, and the cross-section of a HAm showing the initial HA particles can be observed from Fig. 7c to Fig. 7f.

Regarding the residual moisture of powders obtained at different times, the moisture percentage values oscillated in a range between 1.5% and 0.6%. This tolerable variation of less than 1% on the powder humidity led us to assume that the steady-state regime of the process was rapidly reached and no longer operation times are required.

To conclude this preliminary study of the SD process time influence on particles morphology, not important differences between the obtained HAm morphologies, sizes and humidities at different process times were found during the first two hours; demonstrating that the steady-state regime of the process is rapidly reached. Thus, it was chosen to characterize the following experimental runs performed in this study at a same duration time of 20 min for better comparison. Since the presence of a small percentage of mushroom/convex/doughnut particles in a PBSLP powder feedstock has not been demonstrated to have an unfavourable effect, the variables involved in their production have not been further investigated.

Once the time required to reach the steady-state of the process has been evaluated, the effect of the different operating conditions on the product quality was carried out. Hence, the following study was focused on the analysis of HAm morphology in terms of mean particle size and their PSD only.

### *3.2.2. Influence of the parameters of the spray-drying process on the properties of the powders*

First, experiments with different combinations of operating parameters, such as, feed rate, solid mass fraction, spray air pressure, and inlet temperature were performed and the powder obtained was analysed for comparison of average particle size (Fig. 8). The PSD of the powders are offered in (Fig. S1).

It can be observed that the different SD process conditions have an important effect on the final powder size distributions. The most significant impact observed in the parameters studied ranges came from the feed rate (runs 1, 4 and 5) and the temperature of the process (runs 1, 10 and 11).

At similar SD conditions, an increase of feed rate from 3.2 $kg.h^{-1}$ (run 1) to 5.8 $kg.h^{-1}$ (run 5) means almost the double of matter sprayed per hour and in consequence, bigger droplets are formed producing larger average particle size. Same reasoning could have the increase of the average particle size with a higher solid mass fraction on the suspension. A higher amount of HA precursor particles per droplet produces the increase of the final particle size. This direct proportional relation between the droplet size and the feed rate/solid mass fraction operating parameters was already mentioned in literature [5,49]. Furthermore, the purpose of the atomization air pressure is to be able to change the shape of the spray cone and the size of the droplets. And so, it is also clearly observed (runs 1, 6 and 7) that a higher spray air pressure producing finer droplets reduces the average size of the formed agglomerates [5,49,50].

The inlet temperature is known to affect the final particle size in different ways [5,51]. A rise of the temperature reduces the slurry surface tension, expanding in consequence the droplets and dried particles size. The runs 1, 10, and 11 performed at different inlet temperatures from 250 °C to 300 °C showed an increase of the average particle size. However, the SEM analysis performed on these powders (Fig. 9) showed the apparition of large particles with irregular shape when the inlet temperature was too high (Fig. 9b, run 11). A higher temperature and a shorter drying time do not allow the correct organization of the particles forming the agglomerates. Thus, inducing an irregular shape and an increase of the agglomerates size, then in the runs 1 and 10 the critical temperature value was not exceeded and the formation of particles with irregular shape was avoided giving, as a result, the production of HAm (Fig. 9a).

It was already observed that the addition of PVA to the suspensions did not suppose a high increase of the suspension viscosity (viscosity <0.1 Pa.s for the evaluated shear rate range 1–1000 $s^{-1}$) that could lead to handling problems during the spray-drying process, especially during the pumping and mixing of the slurry. The spray-drying processing of ceramic suspensions using PVA as binder during the granule formation was possible.

The addition of PVA (runs 1, 8 and 9) acting as binder in a range of 0–5 wt% did not show any apparent effect on the median particle size

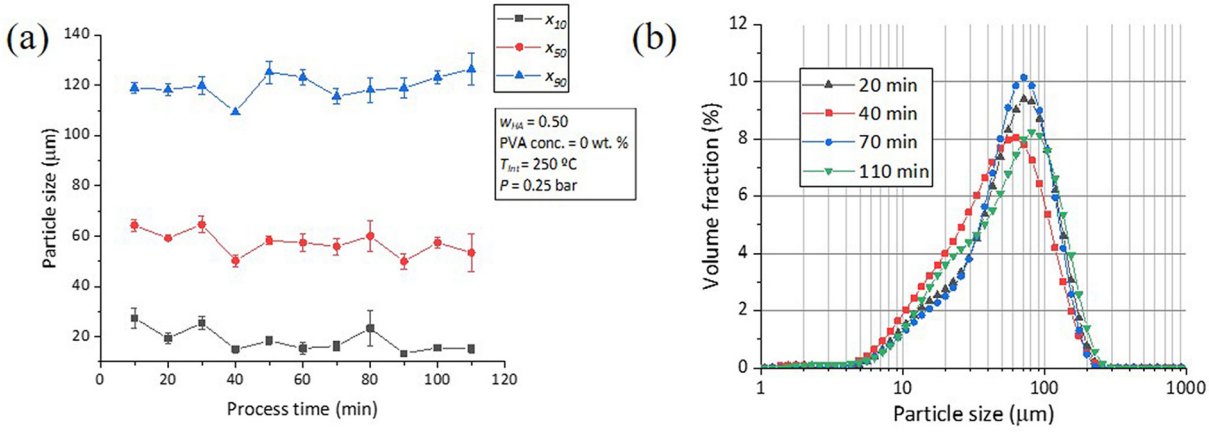


**Fig. 5.** (a) Average particle size ($x_{10}$, $x_{50}$, and $x_{90}$) of powders obtained at different process times and (b) PSD of the powders obtained at 20, 40, 70, and 110 min.

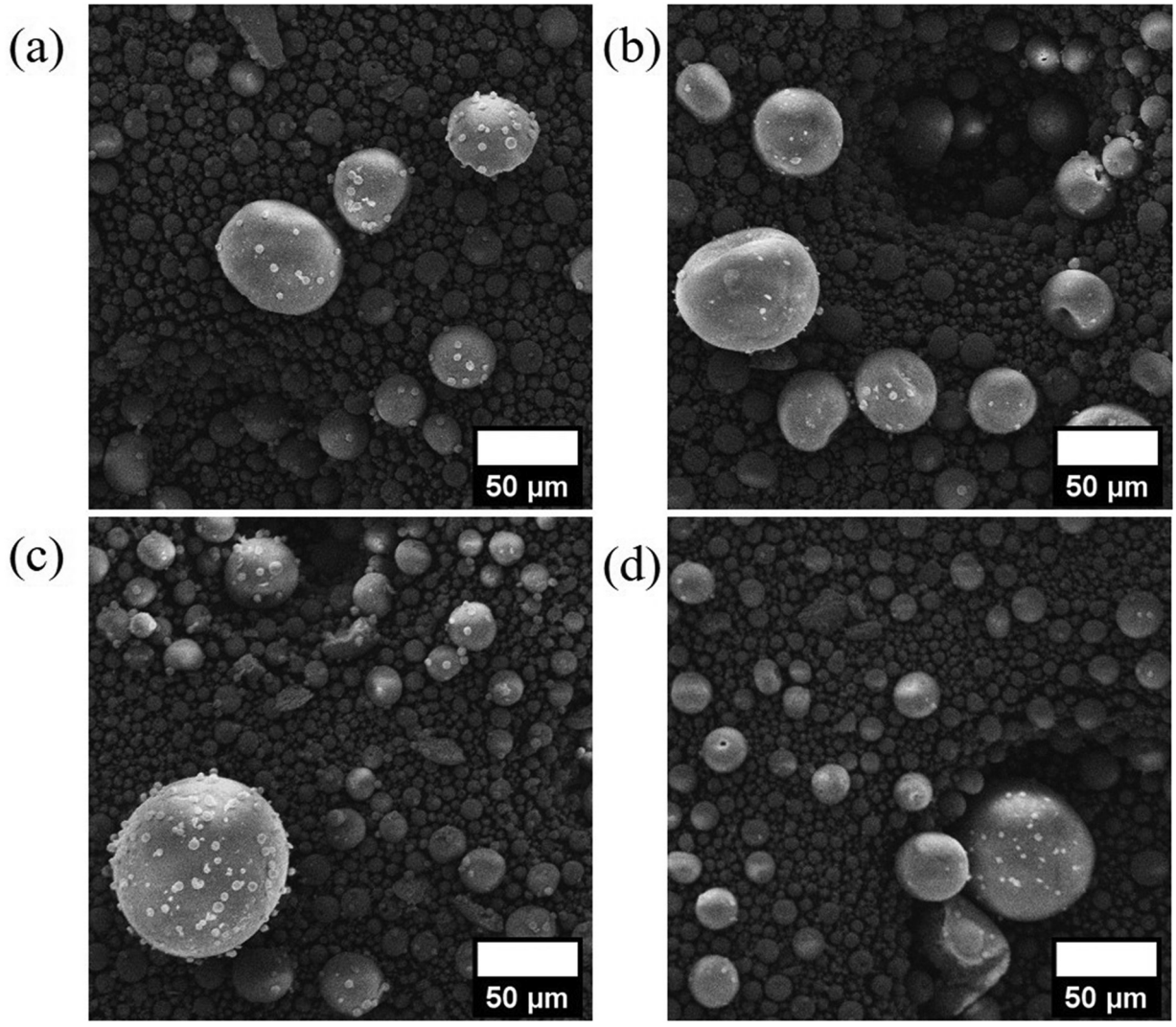


**Fig. 6.** SEM micrographs of spray-dried HAm at (a) 20 min, (b) 60 min, (c) 90 min, and (d) 110 min of process time.

of the spray-dried HAm (Fig. 10a). However, the addition of PVA seemed to reduce the population of particles with a $x_{50}$ = 15–20 μm. This could indicate a favouring of the formation of the HAm of larger size during the SD process or the enhancement of their hardness. A preliminary analysis of the mechanical properties of the HAm obtained was possible by using different dispersion pressures during the particle size analysis by laser diffraction in a dry way. It was observed that the granules spray-dried with a slurry free of PVA were more fragile and were more affected by the increase of the dispersion pressure reducing their particle size (Fig. 10b). More than a 50% of average particle size diminution was observed for the powder without PVA when the dispersion pressure was increased from 0.1 bar to 4 bar, while the powders containing PVA decreased their size a 25%.

A higher residual moisture was observed on spray-dried powders in presence of PVA (runs 8 and 9) showing moisture content values in between 4 and 5%. While in absence of PVA (rest of experimental runs), lower moisture content values ranging 1–2% were observed. This could be due to a higher water retaining in the structure of the agglomerates by the polymeric binder, but this increase of residual moisture should not affect their performance in a PBSLP apparatus. We could conclude that the addition of a binder such as PVA can improve the granules breakage resistance if the intended application requires it without any important alteration of the powder properties such as the PSD.

*3.2.3. Spray-drying operating parameters optimization*

An additional study was performed to find a more optimal SD operating parameters combination for better process efficiency, what is to say, reaching a higher recovery rate (process performance) but keeping in mind that the particles must have the required properties of size, shape and flowability targeted for AM. An increase of the feed rate could make difficult the atomization of too large droplets, since it could cause an insufficient drying rate when the inlet temperature is not high enough, reducing the recovery rate. For this reason, several experiments (runs 12, 13 and 14) were performed at experimental conditions where both, the feed rate and the inlet temperature were increased accordingly. Fig. 11a shows the PSD and average particle size comparison between the three runs at different SD operating parameters sets (feed rates and temperatures). A slight increase of the average particle size is observed on the runs using higher feed rate and inlet temperature. In terms of particles morphology there were no significant differences between them, showing all of them a predominance of the already seen HAm, also defined as, small rough spherical dense particles. SEM micrographs were obtained from runs 13 and 14 and they can be observed in Fig. 11b and Fig. 11c, respectively, showing no critical differences in terms of particles morphology.

For all the experiments, the recovery rate is understood as the yield of dry HA powder recovered in the collection jar at the end of the process respect to the solid mass within the spray-dried slurry. It was

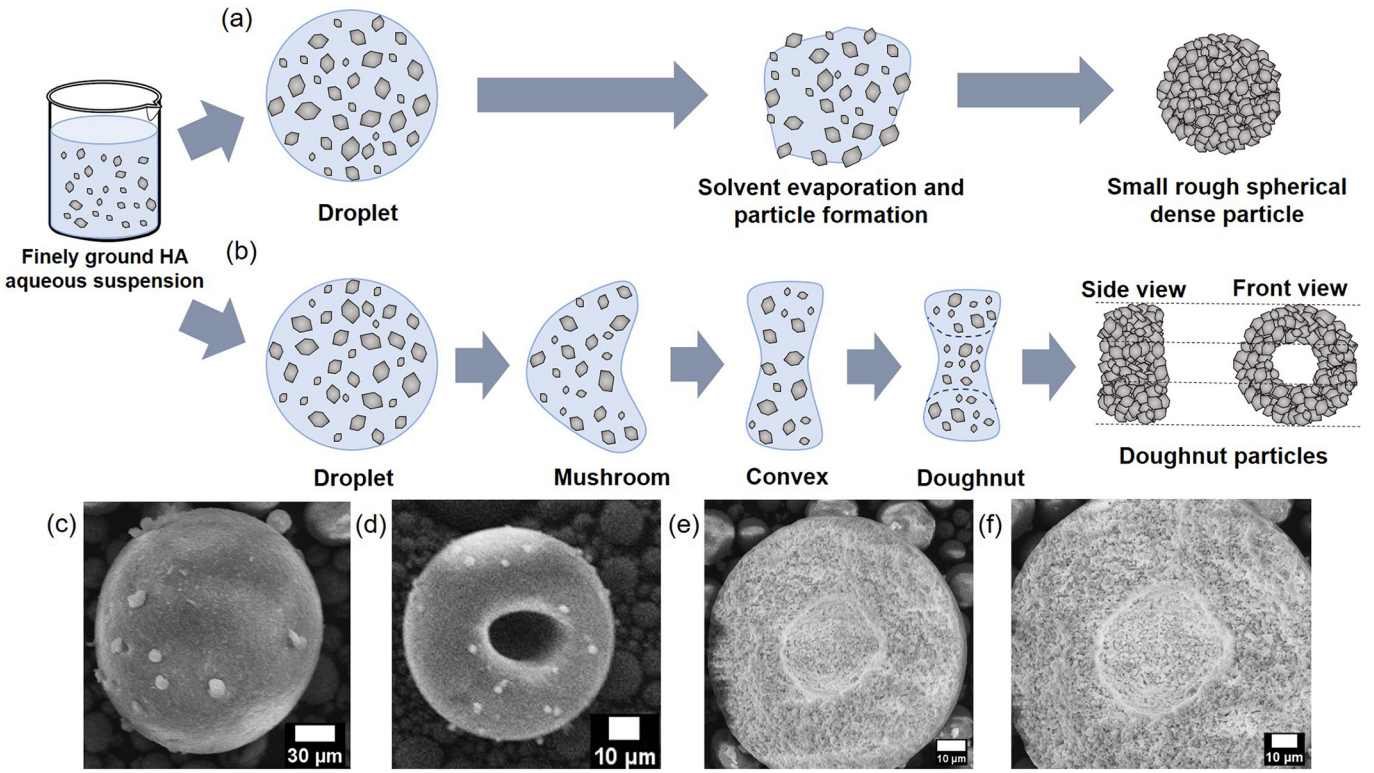


**Fig. 7.** Formation mechanism of (a) small rough spherical dense particles and (b) mushroom, convex, and doughnut particles (based on Okuyama et al. [2]). SEM micrographs of spray-dried (c) small rough HAm, (d) doughnut HA particle produced at specific conditions, (e) cross-section of a HAm showing the initial HA particles forming the agglomerate and (f) at higher magnification.

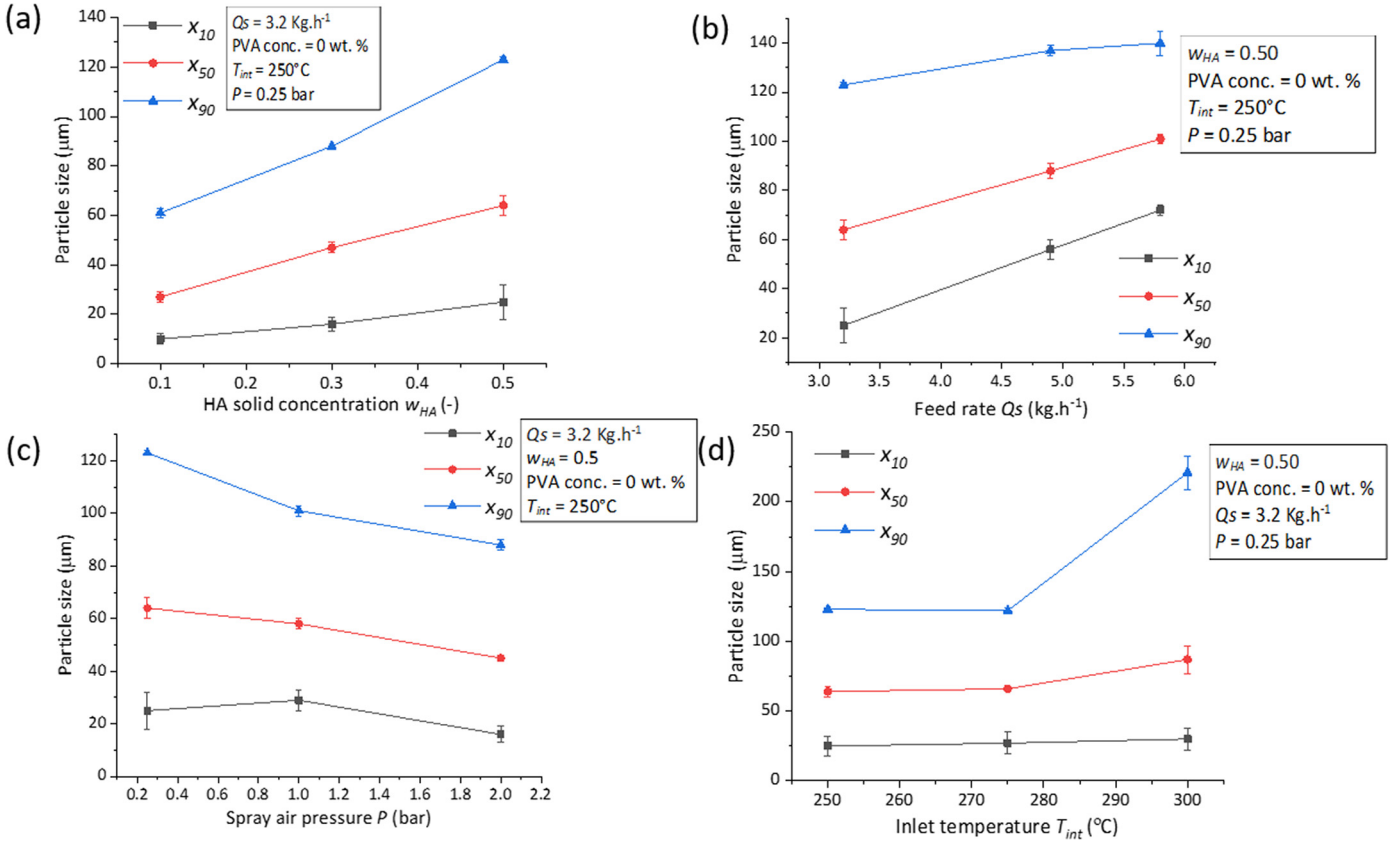


**Fig. 8.** Main spray-dryer operating parameters effect on HAm average particle size ($x_{10}$, $x_{50}$, and $x_{90}$). (a) Solid mass fraction (runs 1-2-3), (b) feed rate (runs 1-4-5), (c) spray air pressure (runs 1-6-7), and (d) inlet temperature (runs 1-10-11).

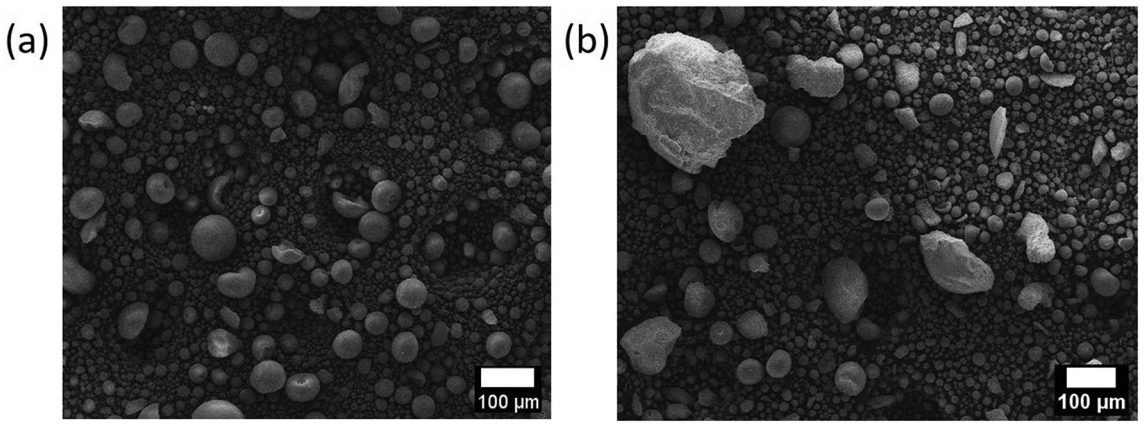


**Fig. 9.** SEM micrographs of (a) HAm formed at inlet temperature of 275 °C (run 10), (b) powder at inlet temperature of 300 °C (run 11) with irregular shape particles.

observed that the operating parameters of the SD process influence the recovery percentage. Recovery rates of all experiment runs are summarized in Fig. 12. A clear tendency to obtain higher recovery rate is observed when using higher spray air pressure (runs 6 and 7). In addition, feed rate and inlet temperature play an important role to obtain a higher recovery rate. The highest recovery rates were obtained when, at high spray air pressure, the feed rate and the inlet temperature were increased accordingly (runs 12, 13, and 14), thus reaching the highest evaporation rate (amount of slurry evaporated per hour). Run 12 reached the highest recovery rate of this study with a value of 79%.

### 3.3. Powders characterization

#### 3.3.1. Flowability of powders

In this section, powders flowability, packing density, and physico-chemical properties were evaluated before and after the SD process to

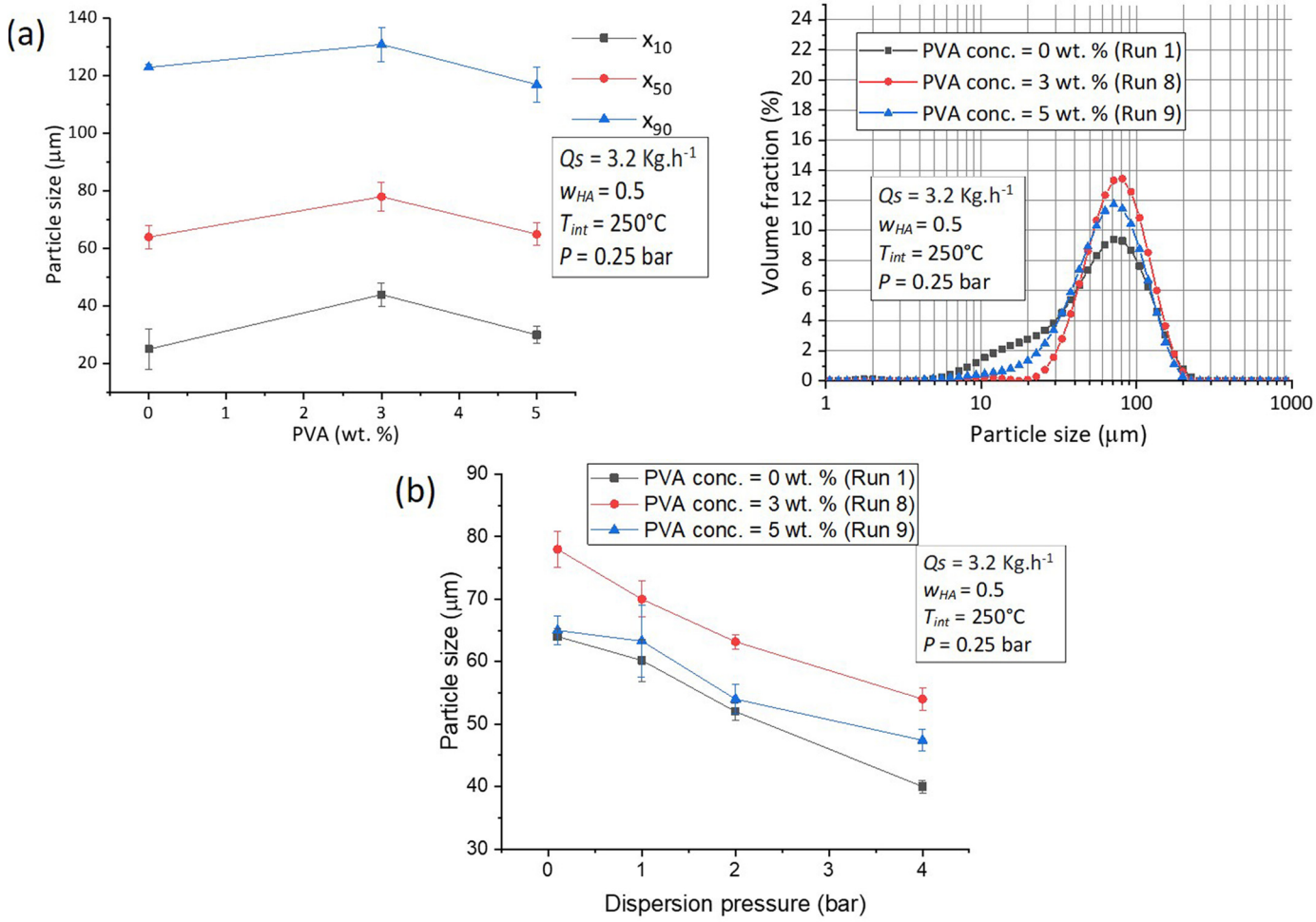


**Fig. 10.** (a) Average particle size and PSD of spray-dried HA powders depending on slurry PVA binder concentration (Runs 1, 8, and 9). (b) Average particle size evolution of previous spray-dried powders at different dispersion pressures during the particle size analysis.

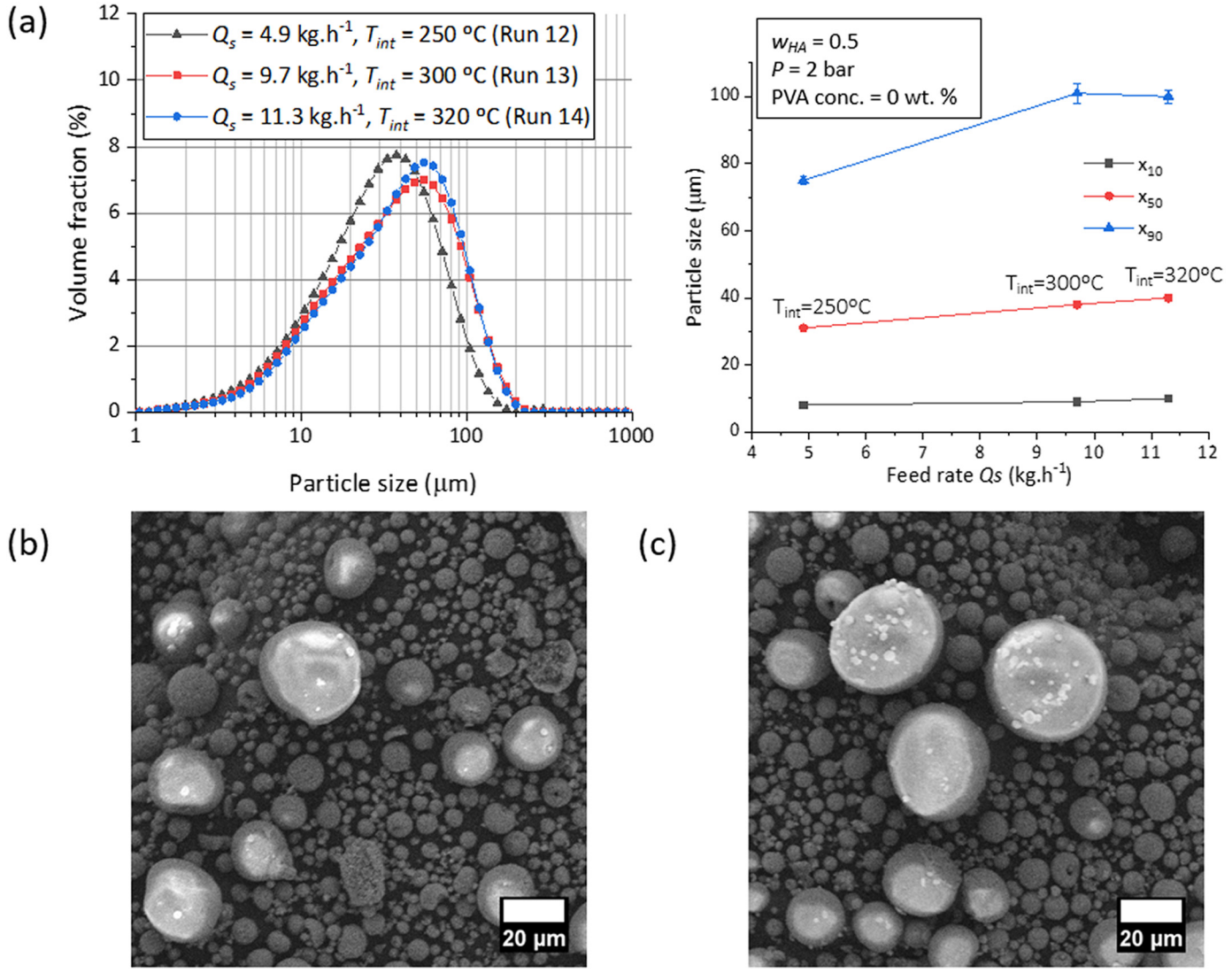


**Fig. 11.** (a) PSD and average particle size of HA powders produced with the most efficient SD operating parameters sets (Runs 12, 13, and 14). SEM micrographs of HA powders produced at different combinations of feed rate and inlet temperature (a) Qs = 9.7 kg.h$^{-1}$, $T_{int}$ = 300 °C (run 13) and (b) Qs = 11.3 kg.h$^{-1}$, $T_{int}$ = 320 °C (run 14).

ensure that their flowability is improved and their material integrity remains unaltered during the process.

The importance of having a good powder flow behaviour is due to its direct impact on the homogeneity of a spread powder bed in a PBSLP apparatus. The quality of the powder bed influences the density of the printed parts [8]. Different recoating devices have been evaluated for the powder bed deposition onto the building platform before laser scanning, e.g., blades (with different shapes), scrapers or rotating roller [52,53]. It was found that a lower surface roughness in the powder bed is better achieved when using a combination of flat-shaped blade and counter-rotating roller, which produce even compaction of the particles, although it needs a deeper study [54]. Recently, the importance of the powder bed compaction just after its spreading and prior laser scanning has been confirmed as an influencing parameter for the improvement of the surface finishing of the ceramic calcium phosphate printed parts [55]. This opens a new discussion about the benefits of having breakable agglomerated particles that will produce a higher packing density of the powder bed after roller compaction.

A deeper description of the different powder flowability measurement techniques (static and dynamic) to determine the flow behaviour of powders was offered by Spierings et al. [17]. It does not exist a single technique suitable for a complete characterization of a powder flow, so

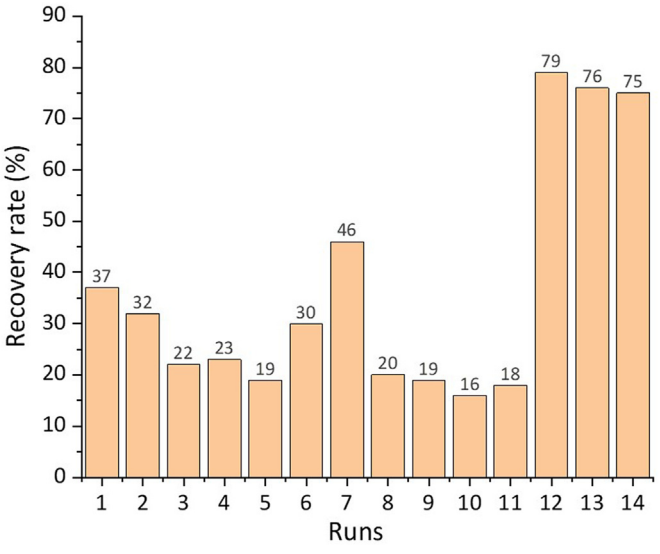


**Fig. 12.** HA powder recovery rate of runs at different SD operating parameters.

different approaches have to be used. The method used should match as much as possible the powder dynamics during its application to have the closest approximation to the reality [56]. The minimum limits for the flowability requirements are highly influenced by the PBSLP apparatus design and the type of layer creation device.

PSD and morphology of powders have an important effect on flowability of powders. In literature, different works have exposed that for powders of narrow PSD the most spherical and larger the particles, the better they flow [19–22]. Between powders with different level of PSD dispersion, a higher dispersion improves the flowability and packing density of the powder. In bimodal size distributions, the smaller particles fill the interstitial voids between the larger particles. A weight fraction of coarse particles about 70% is the condition showing maximum packing density [23–25].

In this study, three different powders were evaluated in terms of flowability. Initial HA powder before the SD process, spray-dried HAm produced following the conditions described in the run 1, and commercial HA powder 300–08-2 from Urodelia®. Between all spray-dried samples, the flowability measurements were only performed on the powder from run 1 due to the quantity of powder available. This powder will thus be considered as relatively representative of the majority of powders recovered during the various runs (for those with mean size and span properties within the required range).

SEM micrographs of the spray-dried HAm were already shown previously (Fig. 6), while the micrographs of the commercial and initial powders can be seen in Fig. 13. Both commercial HA and the HAm produced in the present study have spherical shape due to the spray-drying step carried out as part of their production process. It is not the case of the initial dry powder which shows an irregular shape. This last powder has a tendency to agglomerate when dry, and an additional hand-crushing step was needed to homogenize it.

Table 3 shows a summary of the properties of the three powders (Initial HA, spray-dried HAm, and commercial HA powder) that were evaluated with the different flowability tests. Between both spray-dried powders, the one produced during the run 1 in the present study and the powder from Urodelia®, the differences in flowability are less notorious and the powder that shows the best flowability is dependant of the flowability test. The results obtained from the angle of repose and flow rate tests indicate that the spray-dried powder from the present study could have a better performance than the commercial powder. However, the Hausner ratio suggests that these two are very close in flowability, slightly better in the commercial one. Only in the case of the flow factor analysis, the initial powder takes the first position as the most flowable, although the three of them are classified as free flowing powders.

If we consider that static and dynamic characterization techniques do not necessarily agree, for example, powders showing good fluidization performance can also show agglomeration. It means that flow properties depend on the stress state and that there is no unique technique suitable for a complete characterization of a powder. Both types of procedures, static (e.g., flow factor, compressibility, and Hausner ratio) and dynamic (e.g., flow rate) should be used to fully understand the flow behaviour of a powder [56]. In the case of the angle of repose technique, it combines both static and dynamic elements and it is a standard test for quality control allowing a quick comparison between flow properties of powders [56]. In this case, the flow rate technique has a closer powder dynamic to the recoating process in a PBSLP additive manufacturing apparatus. Then we could consider it the most accurate method to evaluate the performance of the powders for a use as PBSLP powder feedstock.

### 3.3.2. Physico-chemical properties of powders

To discard any possible alteration in the properties of the product, for example due to a phase transition or to any kind of contamination during the process, different physico-chemical analyses of the products were performed. Fig. 14 shows the XRD spectra comparison between the initial HA powder and the powder once it has been spray-dried (run 1). A particular increase of the powder crystallinity (narrower peaks) was observed for the powder after the SD process. No phase transition of the initial calcium phosphate phase (stoichiometric hydroxyapatite (JCPDS 00–009-0432)) was appreciated on the spectrum after the process [57].

The FTIR spectra of the powder before and after the SD process are shown in Fig. 15. There was no presence of side compounds that could be produced during the SD process. Then, as for XRD analysis, the FTIR method confirmed that the physico-chemical integrity of the material remains nearly unaltered.

$PO_4$ and $OH^-$ vibration bands are visible at 1092 $cm^{-1}$, 1040 $cm^{-1}$, 962 $cm^{-1}$, 601 $cm^{-1}$, 575 $cm^{-1}$, 561 $cm^{-1}$, and at 650 $cm^{-1}$, 3600 $cm^{-1}$, respectively [57,58]. In the spray-dried powder spectrum, a weak, almost invisible band corresponding to water absorbed (3400 $cm^{-1}$) is observed confirming the low moisture present powder. A very weak band can be observed at 1400 $cm^{-1}$ in initial HA powder which could correspond with a low presence of dispersant DC used in the suspension feedstock [59]. Then, the filtering and washing steps to obtain the initial dry powder could not be enough to remove the dispersant completely. However, this band becomes nearly invisible after the SD process, indicating a more evident elimination of the dispersant during the process, which could be due to thermal degradation.

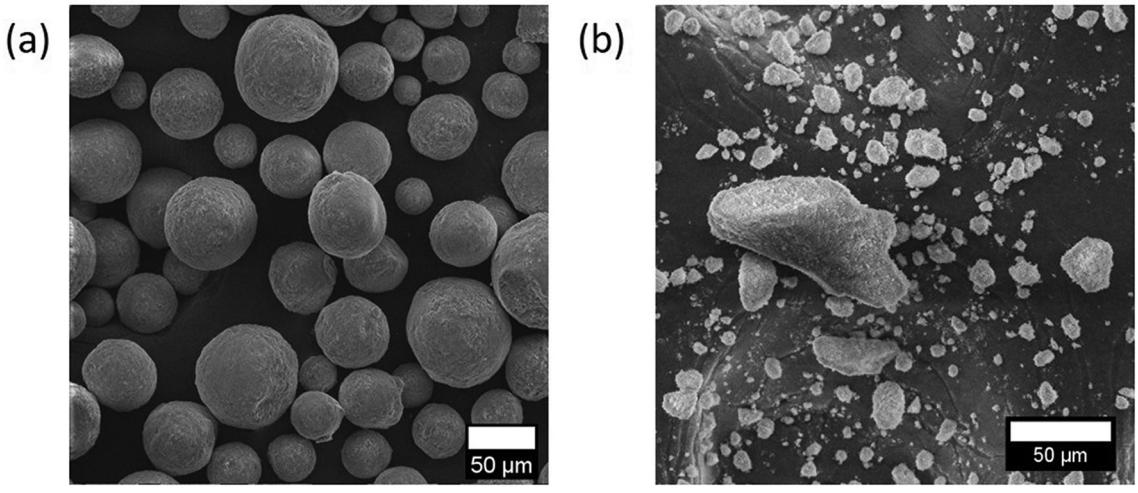


**Fig. 13.** (a) Commercial Urodelia® 300–08-2 powder and (b) dry initial HA powder SEM micrographs.

**Table 3**
Flowability measurements of HA powders in the present study for comparison. Standardized methods according to the European Pharmacopoeia Chapter 2.9.36.

| | Powder characteristics | | Flowability tests results | | | | |
|---|---|---|---|---|---|---|---|
| HA Powder sample | $x_{50}$ (μm) | Span | Angle of repose α (°) | Compressibility index (%) | Hausner ratio *HR*(−) | Flow rate (kg.h$^{-1}$) | $ff_c$ (−) |
| Initial HA (filtered and dry) | 44 ± 5 | 11.20 | 41.1 ± 1.93 | 27.62 ± 1.20 | 1.380 ± 0.021 | 86.9 ± 17.53 | 22.3 ± 2.4 |
| Spray-dried HAm (Run 1) | 64 ± 4 | 1.77 | 26.5 ± 2.27 | 10.95 ± 0.56 | 1.123 ± 0.007 | 344.6 ± 27.7 | 21;4 ± 2.3 |
| Urodelia® 300–08-2 | 70 ± 5 | 0.92 | 30.9 ± 0.90 | 10.68 ± 1.67 | 1.120 ± 0.021 | 274.9 ± 21.8 | 15.9 ± 2.4 |

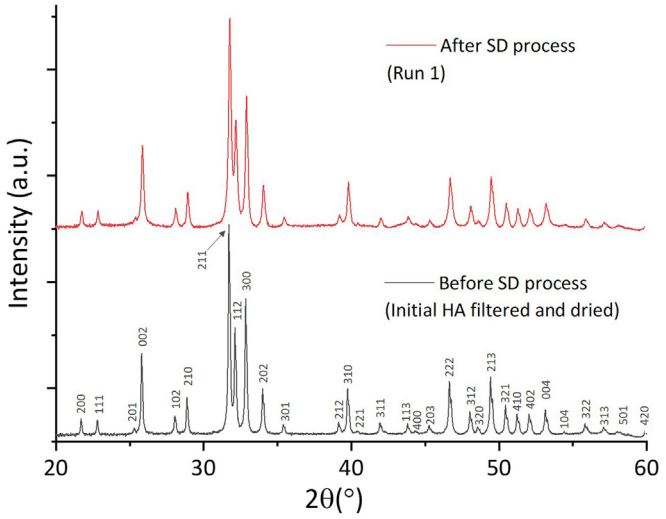


**Fig. 14.** XRD spectrum analysis of the HA before and after the SD process. All the diffraction peaks correspond to stoichiometric hydroxyapatite (JCPDS 000090432).

This section allowed us to emphasize using a SD process to obtain HAm composed powder able to fulfil the flowability requirements in a PBSLP process. The comparison of the produced powder with the initial powder and an already commercial flowable powder made possible to evaluate the quality of our final product. The production of powder with a suitable flowability was then possible by SD process while the physico-chemical properties of the material remained unaltered and no presence of relevant contamination was observed.

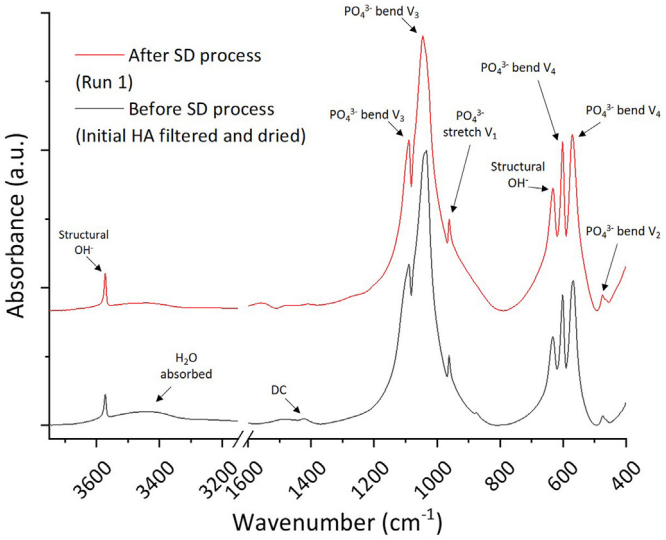


**Fig. 15.** FTIR spectrum analysis of the HA before and after the SD process.

## 4. Conclusions

This paper discussed the effect of the SD process conditions concerning the slurry formulation and experimental parameters on the HAm size and morphology. PVA was demonstrated to be effective as binder improving the dry agglomerates breakage resistance without a significant increase of suspension viscosity. The results indicated that the feed rate and solid mass fraction showed the highest effect on the morphology of spray-dried particles, obtaining larger average particle size when they are increased. It exists a critical value for the inlet temperature with respect to the feed rate and when it is exceeded, the morphology of the particles is altered producing particles with irregular shape. HA microspheres were the main morphology obtained during the process for temperatures under this limit. Several parameters set allowed us to obtain the targeted HAm particle size of 30 μm $< x_{50} <$ 70 μm with a size distribution span higher than 1. However, the highest powder recovery rate values were obtained when using high spray air pressure together with high feed rate and temperature. It was demonstrated that the targeted powder properties help to fulfil the flowability requirements for its use as PBSLP powder feedstock through comparison with different powders. Moreover, the physico-chemical properties of the powder were not altered during the SD process. This study allowed us to develop a quantitative relationship between powder morphology and SD process conditions while confirming that this is a promising process for the production of HAm with suitable properties for the PBSLP technology.

Supplementary data to this article can be found online at https://doi.org/10.1016/j.powtec.2022.117116.

## Declaration of Competing Interest

The authors declare that they have no known competing financial interests or personal relationships that could have appeared to influence the work reported in this paper.

## Acknowledgments

This project has received funding from the European Union's Horizon 2020 research and innovation programme under the Marie Skłodowska-Curie grant agreement No 764935.

## References

[1] A. Stunda-Zujeva, Z. Irbe, L. Berzina-Cimdina, Controlling the morphology of ceramic and composite powders obtained via spray drying – a review, Ceram. Int. 43 (2017) 11543–11551, https://doi.org/10.1016/j.ceramint.2017.05.023.

[2] A.B.D. Nandiyanto, K. Okuyama, Progress in developing spray-drying methods for the production of controlled morphology particles: from the nanometer to submicrometer size ranges, Adv. Powder Technol. 22 (2011) 1–19, https://doi.org/10.1016/j.apt.2010.09.011.

[3] R.P. Patel, Spray drying technology: an overview, IJST. 2 (2009) 44–47, https://doi.org/10.17485/ijst/2009/v2i10.3.

[4] E. Kusrini, A.R. Pudjiastuti, S. Astutiningsih, S. Harjanto, Preparation of Hydroxyapatite from Bovine Bone by Combination Methods of Ultrasonic and Spray Drying, 2012 5.

[5] F.E. Bastan, G. Erdogan, T. Moskalewicz, F. Ustel, Spray drying of hydroxyapatite powders: the effect of spray drying parameters and heat treatment on the particle size and morphology, J. Alloys Compd. 724 (2017) 586–596, https://doi.org/10.1016/j.jallcom.2017.07.116.

[6] Q. Murtaza, J. Stokes, M. Ardhaoui, Experimental analysis of spray dryer used in hydroxyapatite thermal spray powder, J. Therm. Spray Technol. 21 (2012)https://doi.org/10.1007/s11666-012-9791-9.

[7] N. Eliaz, N. Metoki, Calcium phosphate bioceramics: a review of their history, Struct. Prop. Coat. Technol. Biom. Appl. Mater. 10 (2017) 334, https://doi.org/10.3390/ma10040334.

[8] D. Grossin, A. Montón, P. Navarrete-Segado, E. Özmen, G. Urruth, F. Maury, D. Maury, C. Frances, M. Tourbin, P. Lenormand, G. Bertrand, A review of additive manufacturing of ceramics by powder bed selective laser processing (sintering / melting): calcium phosphate, silicon carbide, zirconia, alumina, and their composites, Open Ceramics. 5 (2021) 100073, https://doi.org/10.1016/j.oceram.2021.100073.

[9] Y. Xia, P. Zhou, X. Cheng, Y. Xie, C. Liang, C. Li, S. Xu, Selective laser sintering fabrication of nano-hydroxyapatite/poly-ε-caprolactone scaffolds for bone tissue engineering applications, Int. J. Nanomedicine 8 (2013) 4197–4213, https://doi.org/10.2147/IJN.S50685.

[10] S. Eosoly, D. Brabazon, S. Lohfeld, L. Looney, Selective laser sintering of hydroxyapatite/poly-ε-caprolactone scaffolds, Acta Biomater. 6 (2010) 2511–2517, https://doi.org/10.1016/j.actbio.2009.07.018.

[11] F. Cruz, Fabrication of HA/PLLA composite scaffolds for bone tissue engineering using additive manufacturing technologies, in: M. Elnashar (Ed.), Biopolymers, Sciyo, 2010. https://doi.org/10.5772/10264.

[12] B. Duan, M. Wang, W.Y. Zhou, W.L. Cheung, Z.Y. Li, W.W. Lu, Three-dimensional nanocomposite scaffolds fabricated via selective laser sintering for bone tissue engineering, Acta Biomater. 6 (2010) 4495–4505, https://doi.org/10.1016/j.actbio.2010.06.024.

[13] C. Colin, J.-D. Bartout, E. Shaker, Osseomatrix patent - WO2014154901A1, WO2014154901A1, 2014.

[14] C. Shuai, P. Li, J. Liu, S. Peng, Optimization of TCP/HAP ratio for better properties of calcium phosphate scaffold via selective laser sintering, Mater. Charact. 77 (2013) 23–31, https://doi.org/10.1016/j.matchar.2012.12.009.

[15] K. Zeng, D. Pal, B. Stucker, A review of thermal analysis methods in laser sintering and selective laser melting, 23rd Annual International Solid Freeform Fabrication Symposium - An Additive Manufacturing Conference, 2012, SFF 2012, pp. 796–814.

[16] M. Schmid, F. Amado, G. Levy, K. Wegener, Flowability of powders for selective laser sintering (SLS) investigated by round Robin test, in: P. da Silva Bártolo, A. de Lemos, A. Pereira, A. Mateus, C. Ramos, C. Santos, D. Oliveira, E. Pinto, F. Craveiro, H. da Rocha Terreiro Galha Bártolo, H. de Amorim Almeia, I. Sousa, J. Matias, L. Durão, M. Gaspar, N. Fernandes Alves, P. Carreira, T. Ferreira, T. Marques (Eds.), High Value Manufacturing: Advanced Research in Virtual and Rapid Prototyping, CRC Press 2013, pp. 95–99, https://doi.org/10.1201/b15961-19.

[17] A.B. Spierings, M. Voegtlin, T. Bauer, K. Wegener, Powder flowability characterisation methodology for powder-bed-based metal additive manufacturing, Prog. Addit. Manuf. 1 (2016) 9–20, https://doi.org/10.1007/s40964-015-0001-4.

[18] G.V. Barbosa-Cánovas (Ed.), Food Powders: Physical Properties, Processing, and Functionality, Kluwer Academic/Plenum Publishers, New York, 2005.

[19] H. Lu, X. Guo, Y. Liu, X. Gong, Effect of particle size on flow mode and flow characteristics of pulverized coal, KONA. 32 (2015) 143–153, https://doi.org/10.14356/kona.2015002.

[20] L.X. Liu, I. Marziano, A.C. Bentham, J.D. Litster, E.T. White, T. Howes, Effect of particle properties on the flowability of ibuprofen powders, Int. J. Pharm. 362 (2008) 109–117, https://doi.org/10.1016/j.ijpharm.2008.06.023.

[21] X. Fu, D. Huck, L. Makein, B. Armstrong, U. Willen, T. Freeman, Effect of particle shape and size on flow properties of lactose powders, Particuology. 10 (2012) 203–208, https://doi.org/10.1016/j.partic.2011.11.003.

[22] M.K. Stanford, C. Dellacorte, D. Eylon, Particle size effects on flow properties of Ps304 plasma spray feedstock powder blend, in: W.M. Kriven, H.-T. Lin (Eds.), Ceramic Engineering and Science Proceedings, John Wiley & Sons, Inc., Hoboken, NJ, USA 2003, pp. 577–585, https://doi.org/10.1002/9780470294802.ch82.

[23] D. Sofia, D. Barletta, M. Poletto, Flowability of Ceramic Powders in the Sintering Process, Thapar University, Jaipur (Rajasthan), India, 2016 8.

[24] D. Sofia, R. Chirone, P. Lettieri, D. Barletta, M. Poletto, Selective laser sintering of ceramic powders with bimodal particle size distribution, Chem. Eng. Res. Des. 136 (2018) 536–547, https://doi.org/10.1016/j.cherd.2018.06.008.

[25] N.P. Karapatis, G. Egger, Optimization of Powder Layer Density in Selective Laser Sintering, in: AUSTIN, TX, 1999 10.

[26] D. Yan, B. Zeng, Y. Han, H. Dai, J. Liu, Y. Sun, F. Li, Preparation and laser powder bed fusion of composite microspheres consisting of poly(lactic acid) and nano-hydroxyapatite, Add. Manufact. 34 (2020) 101305, https://doi.org/10.1016/j.addma.2020.101305.

[27] A. Krokos, A. Bondyra, R. Kwiatkowski, P. Gruber, M. Olejarczyk, B. Stępak, P. Dzienny, B. Kryszak, M. Gazińska, A. Antończak, Comparison of thermal, structural and morphological properties of poly(l-lactide) and poly(l-lactide)/ hydroxyapatite microspheres for laser sintering processes, Polimery. 65 (2020) 605–612, https://doi.org/10.14314/polimery.2020.9.2.

[28] C. Esposito Corcione, F. Gervaso, F. Scalera, S.K. Padmanabhan, M. Madaghiele, F. Montagna, A. Sannino, A. Licciulli, A. Maffezzoli, Highly loaded hydroxyapatite microsphere/ PLA porous scaffolds obtained by fused deposition modelling, Ceram. Int. 45 (2019) 2803–2810, https://doi.org/10.1016/j.ceramint.2018.07.297.

[29] Y. Wang, W. Xu, Y. Lu, W. Xu, H. Yin, G. Xiao, Investigation of nature of starting materials on the construction of hydroxyapatite 1D/3D morphologies, Mater. Sci. Eng. C 108 (2020) 110408, https://doi.org/10.1016/j.msec.2019.110408.

[30] S. Mishra, T.R. Rautray, Silver-incorporated hydroxyapatite–albumin microspheres with bactericidal effects, J. Korean Ceram. Soc. 57 (2020) 175–183, https://doi.org/10.1007/s43207-020-00018-z.

[31] S.H. Daryan, A. Khavandi, J. Javadpour, Surface engineered hollow hydroxyapatite microspheres: hydrothermal synthesis and growth mechanisms, Solid State Sci. 106 (2020) 106301, https://doi.org/10.1016/j.solidstatesciences.2020.106301.

[32] H. Huang, M. Du, J. Chen, S. Zhong, J. Wang, Preparation and characterization of abalone shells derived biological mesoporous hydroxyapatite microspheres for drug delivery, Mater. Sci. Eng. C 113 (2020) 110969, https://doi.org/10.1016/j.msec.2020.110969.

[33] H.Y. Yang, M. Wang, Effect of reaction parameters on the thermostability of spray-dried hydroxyapatite powders, Processing and Fabrication of Advanced Materials VIII, WORLD SCIENTIFIC, Singapore 2001, pp. 307–316, https://doi.org/10.1142/9789812811431_0036.

[34] L.C. Chow, L.M. Sun, B. Hockey, Properties of nanostructured hydroxyapatite prepared by a spray drying technique, J. Res. Natl. Inst. Stand. Technol. 109 (2004) 543, https://doi.org/10.6028/jres.109.041.

[35] H. Schappo, K. Giry, C. Damia, D. Hotza, Screening method for producing suitable spray-dried HA powder for SLS application, Powder Technol. 384 (2021) 62–69, https://doi.org/10.1016/j.powtec.2021.02.004.

[36] P. Navarrete-Segado, C. Frances, M. Tourbin, D. Grossin, Powder bed selective laser process (sintering/melting) applied to tailored calcium phosphate-based powders, Addit. Manuf. 50 (2022) 1–20, https://doi.org/10.1016/j.addma.2021.102542.

[37] H. Ji, H.M. Lim, Y.-W. Chang, H. Lee, Comparison of the viscosity of ceramic slurries using a rotational rheometer and a vibrational viscometer, J. Korean Ceramic Soc. 49 (2012), https://doi.org/10.4191/kcers.2012.49.6.542.

[38] D18 Committee, Test Method for Bulk Solids Characterization by Carr Indices, ASTM International, n.d. doi:https://doi.org/10.1520/D6393-14.

[39] Z. Sklubalova, Z. Zatloukal, The influence of orifice height on flow rate of powder excipients, Pharmazie. (2011) 953–955, https://doi.org/10.1691/ph.2011.1074.

[40] A.W. Jenike, Storage and flow of solids, Bulletin No. 123 of the Utah Engineering Experiment Station; Vol. 53, No. 26, November 1964, Utah Univ., Salt Lake City (United States)1976, https://doi.org/10.2172/5240257.

[41] L. Parrella, D. Barletta, R. Boerefijn, M. Poletto, Comparison between a uniaxial compaction tester and a shear tester for the characterization of powder flowability, KONA. 26 (2008) 178–189, https://doi.org/10.14356/kona.2008016.

[42] A. Tsetsekou, C. Agrafiotis, I. Leon, A. Milias, Optimization of the rheological properties of alumina slurries for ceramic processing applications part II: spray-drying, J. Eur. Ceram. Soc. 21 (2001) 493–506, https://doi.org/10.1016/S0955-2219(00)00232-6.

[43] P. Ramavath, R. Papitha, M. Ramesh, P. Babu, R. Johnson, Effect of primary particle size on spray formation, morphology and internal structure of alumina granules and elucidation of flowability and compaction behaviour, PAC. 8 (2014) 93–99, https://doi.org/10.2298/PAC1402093R.

[44] J.S. Reed, J.S. Reed, Principles of Ceramics Processing, 2nd ed Wiley, New York, 1995.

[45] L. Pawlowski, P. Blanchart, Industrial Chemistry of Oxides for Emerging Applications, Wiley, Laboratory SPCTS, University of Limoges, France, 2018.

[46] S. Baklouti, P. Coupelle, T. Chartier, J. Baumard, Compaction behaviour of alumina powders spray-dried with organic binders, J. Phys. III (6) (1996) 1283–1291, https://doi.org/10.1051/jp3:1996186.

[47] V. Naglieri, D. Gutknecht, V. Garnier, P. Palmero, J. Chevalier, L. Montanaro, Optimized slurries for spray drying: different approaches to obtain homogeneous and deformable alumina-zirconia granules, Materials. 6 (2013) 5382–5397, https://doi.org/10.3390/ma6115382.

[48] M. Larsson, A. Hill, J. Duffy, Suspension stability; why particle size, zeta potential and rheology are important, Trans. Nordic Rheol. Soc. 20 (2012) 7.

[49] P. Luo, T.G. Nieh, Preparing hydroxyapatite powders with controlled morphology, Biomaterials. 17 (1996) 1959–1964, https://doi.org/10.1016/0142-9612(96)00019-1.

[50] B. Yu, Y.J. Feng, L.S. Wohn, C. Huang, Y.F. Li, Z. Jia, Spray-drying of alumina powder for APS: effect of slurry properties and drying conditions upon particle size and morphology of feedstock, Bull. Mater. Sci. 34 (2011) 1653–1661, https://doi.org/10.1007/s12034-011-0373-0.

[51] X.Q. Cao, R. Vassen, S. Schwartz, W. Jungen, F. Tietz, D. Stöever, Spray-drying of ceramics for plasma-spray coating, J. Eur. Ceram. Soc. 20 (2000) 2433–2439, https://doi.org/10.1016/S0955-2219(00)00112-6.

[52] S. Haeri, Optimisation of blade type spreaders for powder bed preparation in additive manufacturing using DEM simulations, Powder Technol. 321 (2017) 94–104, https://doi.org/10.1016/j.powtec.2017.08.011.

[53] L. Wang, Z. Zhou, E. Li, H. Shen, A. Yu, Powder deposition mechanism during powder spreading with different spreader geometries in powder bed fusion additive manufacturing, Powder Technol. 395 (2022) 802–810, https://doi.org/10.1016/j.powtec.2021.10.017.

[54] S. Beitz, R. Uerlich, T. Bokelmann, A. Diener, T. Vietor, A. Kwade, Influence of powder deposition on powder bed and specimen properties, Materials. (2019)https://doi.org/10.3390/ma12020297.

[55] P. Navarrete-Segado, C. Frances, M. Tourbin, C. Tenailleau, B. Duployer, D. Grossin, Powder bed selective laser process (sintering/melting) applied to tailored calcium phosphate-based powders, Add. Manufact. 50 (2022) 102542, https://doi.org/10.1016/j.addma.2021.102542.

[56] M. Krantz, H. Zhang, J. Zhu, Characterization of powder flow: static and dynamic testing, Powder Technol. 194 (2009) 239–245, https://doi.org/10.1016/j.powtec.2009.05.001.

[57] C. Rey, C. Combes, C. Drouet, D. Grossin, G. Bertrand, J. Soulié, Bioactive calcium phosphate compounds: physical chemistry, Reference Module in Materials Science and Materials Engineering, Elsevier, 2017. https://doi.org/10.1016/B978-0-12-803581-8.10171-7.

[58] C. Rey, O. Marsan, C. Combes, C. Drouet, D. Grossin, S. Sarda, Characterization of calcium phosphates using vibrational spectroscopies, in: B. Ben-Nissan (Ed.), Advances in Calcium Phosphate Biomaterials, Springer, Berlin Heidelberg, Berlin, Heidelberg 2014, pp. 229–266, https://doi.org/10.1007/978-3-642-53980-0_8.

[59] A.M. Popa, J. Vleugels, J. Vermant, O. Van der Biest, Influence of surfactant addition sequence on the suspension properties and electrophoretic deposition behavior of alumina and zirconia, J. Eur. Ceram. Soc. 26 (2006) 933–939, https://doi.org/10.1016/j.jeurceramsoc.2004.12.023.